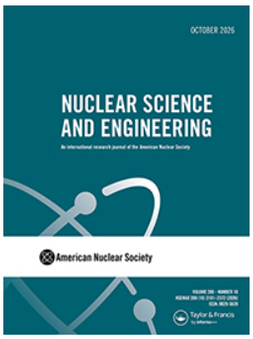

Taylor & Francis
Taylor & Francis Group

Nuclear Science and Engineering

ISSN: 0029-5639 (Print) 1943-748X (Online) Journal homepage: www.tandfonline.com/journals/unse20

Variance Budgeting for Probability Tables in the Unresolved Resonance Region

Alec Golas , Y. Danon , A. M. Lewis & D. Barry

To cite this article: Alec Golas , Y. Danon , A. M. Lewis & D. Barry (11 Aug 2026): Variance Budgeting for Probability Tables in the Unresolved Resonance Region, Nuclear Science and Engineering, DOI: 10.1080/00295639.2026.2706938

To link to this article: https://doi.org/10.1080/00295639.2026.2706938

Published online: 11 Aug 2026.

NUCLEAR SCIENCE AND ENGINEERING

DOI: https://doi.org/10.1080/00295639.2026.2706938

Variance Budgeting for Probability Tables in the Unresolved Resonance Region

Alec Golas[a], Y. Danon[a], A. M. Lewis[b], and D. Barry[c]

[a]*Mechanical, Aerospace, and Nuclear Engineering, Rensselaer Polytechnic Institute, Troy, NY;* [b]*Computational Physics, Los Alamos National Laboratory, Los Alamos, NM;* [c]*Reactor Technology, Naval Nuclear Laboratory, Schenectady, NY*

Received May 1, 2026
Accepted for Publication July 15, 2026

Abstract — *Resonance self-shielding in the unresolved resonance region (URR) is driven by the variance of the cross-section distribution, which probability tables are designed to represent. This paper identifies two mechanisms by which standard nuclear data processing distorts this variance. First, the multiplicative normalization used to enforce mean consistency between the probability table and the evaluated cross section inadvertently rescales the variance. Second, when the evaluated cross section carries resonant structure within a probability table energy bin, the transport code sees both this within-bin structure and the full probability table fluctuation content, double counting the variance. A variance-preserving affine transformation is derived that enforces the evaluated mean while preserving the variance and is extended to a per-reaction variance-budgeting methodology applicable when the evaluated cross section carries within-bin structure. The method is implemented in NJOY/PURR and validated through a controlled ^{235}U transmission study. Integral benchmarks using the HEU-MET-INTER-011 suite show that standard processing overpredicts the URR self-shielding reactivity worth by approximately 150% relative to the variance-preserved result, demonstrating that the effect is quantitatively significant for the ENDF/B-VIII.1 ^{235}U evaluation.*

Keywords — *Unresolved resonance region, probability tables, resonance self-shielding, nuclear data processing.*

I. INTRODUCTION

The energy-dependent structure of neutron cross sections is categorized into distinct regions. Between the resolved resonance region (RRR) and the fast continuum lies the unresolved resonance region (URR), where cross sections possess resonance structure, but individual resonances cannot be resolved experimentally. URR evaluations are therefore limited to average cross sections and average resonance parameters, which are used to describe both the average cross section and the fluctuations around that average, thereby representing the cross section in a statistical manner. These fluctuations must be accounted for in neutron-transmission calculations to obtain physically accurate results. The ratio of the transmission computed with the full fluctuating cross section to that computed using only the average cross section defines the self-shielding correction factor, also referred to as the resonance transmission enhancement.

The standard method to account for URR self-shielding in transport codes is the use of probability tables. These tables provide a discrete probability distribution of cross-section values, generated by statistically sampling many resonance ladders to reflect the underlying fluctuation content. For self-shielding to be physically consistent, the cross-section variance must be accurately reproduced when the probability table is applied in transport.

This paper identifies two distinct mechanisms by which the cross-section variance can be distorted in

CONTACT Alec Golas awgolas@lanl.gov

standard processing workflows. The first is an inadvertent variance scaling that arises when the probability table mean differs from the evaluated File 3 cross-section mean and a multiplicative normalization is used to enforce consistency. The second is a variance double-counting problem that arises when the File 3 cross section carries resonant structure within probability table energy bins while the probability table continues to represent the full fluctuation variance.

These problems are relevant to the transition from ENDF/B-VIII.0 to ENDF/B-VIII.1 [1,2], in which significant resonant structure was introduced into the ^{235}U fission cross section within the URR, making the double-counting problem newly relevant for a major fissile isotope. This paper derives variance-preserving corrections for both problems, implements them in the NJOY2016 processing code, and validates the methodology using controlled transmission tests and integral criticality benchmarks.

II. BACKGROUND

In the ENDF format, a URR evaluation is commonly split between two data files. File 2 provides the average resonance parameters (mean level spacing, average neutron and radiation widths, and their associated degrees of freedom) that encode the compound-nucleus statistical model. File 3 provides the evaluated energy-dependent cross section $\bar{\sigma}(E)$, which serves as the target mean for transport. In general, $\bar{\sigma}$ may include smooth contributions (direct reactions, inelastic thresholds, etc.) that are not represented in the compound-nucleus model.

The processing code PURR [3] uses the File 2 parameters to statistically sample many resonance ladders, producing a discrete probability table at each energy grid point. This table has a sample mean $\hat{\mu}$ and sample variance $\hat{V}$ that estimate the population mean and variance of the underlying cross-section distribution. In general, $\bar{\sigma} \neq \hat{\mu}$, both because $\bar{\sigma}$ may contain smooth contributions absent from the ladder sampling and because the evaluation and processing codes may use different formalisms (for example, Reich-Moore versus single-level Breit-Wigner approximations) to compute the average cross section [4,5].

II.A. Role of Variance in URR Self-Shielding

The purpose of representing the cross-section distribution from the File 2 statistical model (Wigner-distributed level spacings, Porter-Thomas-distributed widths [6]) in transport is to capture resonance self-shielding.

Self-shielding arises because neutron transmission is an exponential function of a highly fluctuating cross section. For a sample with areal number density n, the transmission at a single energy is $T(E) = e^{-n\sigma(E)}$. Because this function is nonlinear, averaging the transmission over a finite energy bin is not the same as computing the transmission from the bin-averaged cross section. By applying Jensen's inequality [7] to the convex function $e^{-n\sigma}$,

$$\langle e^{-n\sigma} \rangle \geq e^{-n\langle\sigma\rangle}, \tag{1}$$

with equality only when σ is constant across the bin. In the URR, the cross section fluctuates within every energy bin, so the inequality is strict, and the bin-averaged transmission always exceeds the smooth cross-section result. To quantify the magnitude of the self-shielding effect, it is useful to decompose the cross section at each energy into its bin-averaged value and a deviation:

$$\sigma(E) = \langle\sigma\rangle + \delta\sigma(E), \qquad \langle\delta\sigma\rangle = 0, \tag{2}$$

where angle brackets $\langle\cdot\rangle$ denote energy averaging within the bin. The self-shielding correction factor, defined as the ratio of the true bin-averaged transmission to the transmission computed from the bin-averaged cross section, then takes the form

$$C_T \equiv \frac{\langle e^{-n\sigma}\rangle}{e^{-n\langle\sigma\rangle}} = \langle e^{-n\,\delta\sigma}\rangle, \tag{3}$$

where the second equality follows from substituting Eq. (2) into the numerator and canceling the common factor $e^{-n\langle\sigma\rangle}$. The self-shielding correction factor therefore depends on only the deviations $\delta\sigma$, not on the mean $\langle\sigma\rangle$. Expanding to second order gives [6]

$$C_T \approx 1 + \frac{n^2}{2} V, \qquad V \equiv \langle(\delta\sigma)^2\rangle. \tag{4}$$

Cross-section variance V is therefore the fundamental quantity that drives resonance self-shielding. The mean $\langle\sigma\rangle$ determines the attenuation in the absence of fluctuations, but V alone determines how much the true transmission exceeds the smooth cross-section result.

To identify what determines V, it is necessary to distinguish which contributions to the cross section produce within-bin fluctuations. In the URR, the energy-dependent cross section within a bin can be written as the sum of a compound-nucleus component $\sigma_{\mathrm{CN}}(E)$ and a smooth contribution σ_{direct} [8,9]:

$$\sigma(E) = \sigma_{\mathrm{CN}}(E) + \sigma_{\mathrm{direct}}\,, \tag{5}$$

where only $\sigma_{\mathrm{CN}}(E)$ fluctuates within a bin. The remaining σ_{direct} is a smooth component and contributes to only the energy-averaged mean. This additive decomposition relies on the absence of significant interference between the compound-nucleus and direct reaction amplitudes. Modified Hauser-Feshbach calculations for ^{208}Pb (n,γ) [10] find the interference correction to reach at most a few percent of the compound-nucleus term, and only at the lowest energies where the direct contribution is most competitive relative to the compound-nucleus cross section. This is a worst-case estimate: ^{208}Pb is a doubly-magic nucleus with strong single-particle structure, making it one of the most favorable cases for large direct-capture contributions. Experimental comparisons across ^{40}Ca, ^{58}Ni, ^{89}Y, and ^{206}Pb [11], all nuclei with significant shell structure, confirm that the compound-nucleus and direct-semidirect contributions can be accurately modeled as independent, incoherent contributions. For the heavy deformed actinides that dominate practical URR applications (e.g., ^{235}U, ^{238}U), the direct component is proportionally smaller, and the incoherent approximation is expected to be even more accurate. The within-bin deviation is therefore

$$\delta\sigma(E) = \sigma(E) - \langle\sigma\rangle = \sigma_{\mathrm{CN}}(E) - \langle\sigma_{\mathrm{CN}}\rangle\,, \tag{6}$$

and the variance depends exclusively on the compound-nucleus fluctuations:

$$V = \langle(\delta\sigma)^2\rangle = \langle(\sigma_{\mathrm{CN}} - \langle\sigma_{\mathrm{CN}}\rangle)^2\rangle \equiv V_{\mathrm{CN}}. \tag{7}$$

Adding smooth contributions to the mean, whether from direct capture [12], inelastic channels [13], or doorway-state corrections [14], shifts $\langle\sigma\rangle$ but does not alter $\delta\sigma(E)$ or V. The compound-nucleus fluctuation variance is set entirely by the File 2 statistical parameters (level densities, neutron and radiation widths) and is independent of the File 3 mean. Because V is an absolute quantity determined by the compound-nucleus parameters alone, it does not scale with $\langle\sigma\rangle$; any processing step that ties the variance to the mean introduces a spurious coupling between two physically independent quantities.

Reproducing URR self-shielding therefore requires that transport codes receive both the correct mean $\bar{\sigma}$ (from the evaluated File 3 cross section) and the correct variance V (from the File 2 statistical model) and requires that these two quantities be treated as independent. This independence has a direct consequence for processing: Any step that enforces the evaluated mean $\bar{\sigma}$ must do so without disturbing V. As shown in Sec. II.C, the standard `LSSF = 1` factor format enforces $\bar{\sigma}$ via a multiplicative scaling, which rescales $\delta\sigma$ and therefore distorts V. An additive correction, by contrast, shifts $\langle\sigma\rangle$ while leaving $\delta\sigma$ invariant.

The distinction matters in practice because the evaluated File 3 mean $\bar{\sigma}$ routinely includes smooth contributions that are absent from the compound-nucleus ladder sampling used by PURR to generate probability tables. The sampled mean $\hat{\mu}$ correctly reflects only the compound-nucleus component, while $\bar{\sigma}$ includes both compound-nucleus and smooth contributions. Part of the discrepancy between $\bar{\sigma}$ and $\hat{\mu}$ thus arises from physics that should shift the mean without affecting the variance.

II.B. Probability Table Representation of URR Fluctuations

Probability tables provide a discrete representation of the within-bin distribution of cross sections [15]. In an energy bin, a probability table supplies cross-section values $\{\sigma_j\}$ with probabilities $\{P_j\}$ (typically 20 bins) such that

$$\sum_j P_j = 1\,. \tag{8}$$

Two summary quantities are the sample mean and variance,

$$\hat{\mu} \equiv \sum_j P_j\sigma_j\,, \tag{9}$$

$$\hat{V} \equiv \sum_j P_j(\sigma_j - \hat{\mu})^2\,. \tag{10}$$

As discussed in Sec. II, $\hat{\mu}$ and $\bar{\sigma}$ generally differ. To enforce consistency with the evaluated mean, probability tables are commonly stored as dimensionless factors (`LSSF = 1` in ENDF-6 format terminology [16]):

$$f_j \equiv \frac{\sigma_j}{\hat{\mu}}\,, \tag{11}$$

so that $\sum_j P_j f_j = 1$. During transport, the cross section seen by the transport code is $f_j\,\bar{\sigma}$, which guarantees that the evaluated mean is recovered: $\sum_j P_j f_j\,\bar{\sigma} = \bar{\sigma}$.

A physically consistent treatment must satisfy two conditions simultaneously: (1) the distribution used in transport must reproduce $\bar{\sigma}$ as its mean, and (2) it must preserve the estimated variance $\hat{V}$. The `LSSF = 1` probability table treatment satisfies condition (1) by construction; the following two subsections show how it can violate condition (2).

II.C. Problem 1: Inadvertent Variance Scaling

Substituting $f_j = \sigma_j/\hat{\mu}$ reveals that the reconstructed cross section $f_j\,\bar{\sigma} = \sigma_j\,(\bar{\sigma}/\hat{\mu})$ is a uniform multiplicative scaling of the sampled distribution by $\bar{\sigma}/\hat{\mu}$. Since $\mathrm{Var}(aX) = a^2\mathrm{Var}(X)$, the variance seen by the transport code becomes

$$\mathrm{Var}\left(f_j\,\bar{\sigma}\right) = \left(\frac{\bar{\sigma}}{\hat{\mu}}\right)^2 \hat{V}\,. \tag{12}$$

Whenever $\bar{\sigma} \neq \hat{\mu}$, condition (2) is violated: $\hat{V}$ is inflated or suppressed by the scaling-induced variance $V_{\mathrm{scale}} = [(\bar{\sigma}/\hat{\mu})^2 - 1]\,\hat{V}$. Fig. 1 illustrates this for the ^{235}U fission cross section using the ENDF/B-VIII.0 evaluation, which is chosen here to isolate the multiplicative-scaling effect from the double-counting problem introduced in ENDF/B-VIII.1 (discussed in Sec. II.D). Even for this heavily smoothed evaluation, the two means differ systematically across the URR, producing variance rescaling of up to 40% in some energy bins.

II.D. Problem 2: Variance Double Counting from File 3 Structure

The multiplicative scaling problem described above distorts $\hat{V}$ when $\bar{\sigma} \neq \hat{\mu}$, but even when these means agree, a second source of variance distortion can arise whenever $\bar{\sigma}$ carries resonant structure within a probability table bin.

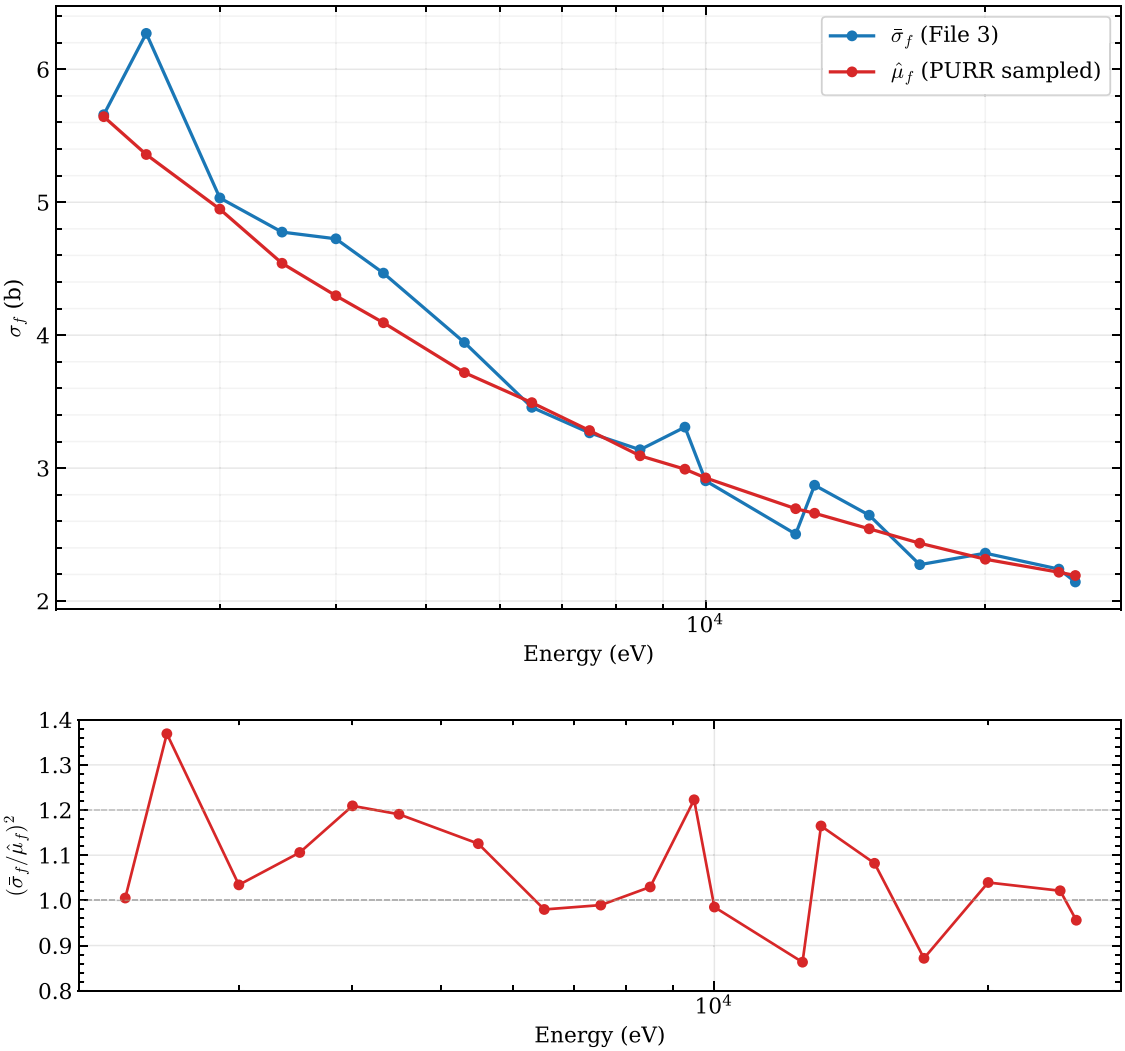

Fig. 1. Inadvertent variance scaling for ^{235}U fission (ENDF/B-VIII.0). (Top) Evaluated mean $\bar{\sigma}_{\mathrm{fis}}$ versus sampled mean $\hat{\mu}_{\mathrm{fis}}$ at each PURR energy grid point. (Bottom) Squared ratio $(\bar{\sigma}_{\mathrm{fis}}/\hat{\mu}_{\mathrm{fis}})^2$, the factor by which the `LSSF = 1` normalization rescales $\hat{V}$ [Eq. (12)]. Deviations from unity indicate spurious variance inflation (>1) or suppression (<1).

Under the standard LSSF = 1 processing workflow, probability tables are generated from the evaluation's average resonance parameters and represent the full estimated variance $\hat{V}$. Separately, $\bar{\sigma}$ provides the evaluated cross section used in transport. If $\bar{\sigma}$ is smooth within each bin, it contributes negligible variance ($V_3 \approx 0$), and the probability table supplies all the fluctuation content, as intended. However, if $\bar{\sigma}$ carries significant resonant structure, the transport code effectively sees *two* sources of within-bin variance: the within-bin variance of $\bar{\sigma}$, denoted V_3, and the full estimated variance $\hat{V}$. The result is a total effective variance of $V_3 + \hat{V}$, which exceeds the intended population variance V and produces excess self-shielding. The ENDF-6 manual anticipates this effect in Sec. 2.4.17, terming it "double-shielding" [16]. Its recommended remedy is to retain File 3 structure only where it reflects a statistically meaningful number of resonances and to smooth the remainder.

II.D.1. Motivating Example: ^{235}U Fission in ENDF/B-VIII.1

The transition from ENDF/B-VIII.0 [1] to ENDF/B-VIII.1 [2] makes this problem concrete. Both evaluations draw on the same experimental fission cross-section dataset [17] but differ in how that data are incorporated into $\bar{\sigma}$. ENDF/B-VIII.0 uses a heavily smoothed representation, retaining only modest within-bin structure ($V_{3,\mathrm{fis}}$ up to ~0.8 b^2 in the lowest-energy bins, decreasing rapidly with energy). ENDF/B-VIII.1 retains substantially more of the measured resonant structure, producing within-bin fission cross-section variance a factor of roughly 3 larger ($V_{3,\mathrm{fis}}$ up to ~2.5 b^2).

Fig. 2 compares $\bar{\sigma}_{\mathrm{fis}}$ across the URR for the two evaluations. Fig. 3 shows the full fission cross-section variance decomposition at each PURR grid point for the ENDF/B-VIII.1 evaluation, quantifying the combined overcounting from V_3 and V_{scale}. At the lowest URR energies, the combined overcounting exceeds 40% of $\hat{V}$. Elastic and capture cross sections are essentially identical between the two evaluations and contribute negligible V_3 in both cases (Fig. 6).

Under the standard processing workflow, the probability tables for both evaluations are generated from the same average resonance parameters using PURR (the File 2 URR parameters are unchanged between ENDF/B-VIII.0 and ENDF/B-VIII.1) and therefore represent the same $\hat{V}$. When the File 3 fission cross section was heavily smoothed (ENDF/B-VIII.0), the standard approach introduced only a small double-counting bias. With the increased fission structure in ENDF/B-VIII.1, $V_{3,\mathrm{fis}}$ becomes a significant fraction of $\hat{V}$, but the probability table factors are not adjusted to account for it. The result is substantial variance double counting for the fission channel. The impact of this overcounting on criticality calculations is quantified in Sec. IV.C.

The two problems identified in Secs. II.C and II.D are related: Both arise from the probability table factor format failing to account for information outside the table itself. Problem 1 ignores the discrepancy between $\hat{\mu}$ and $\bar{\sigma}$. Problem 2 ignores the within-bin

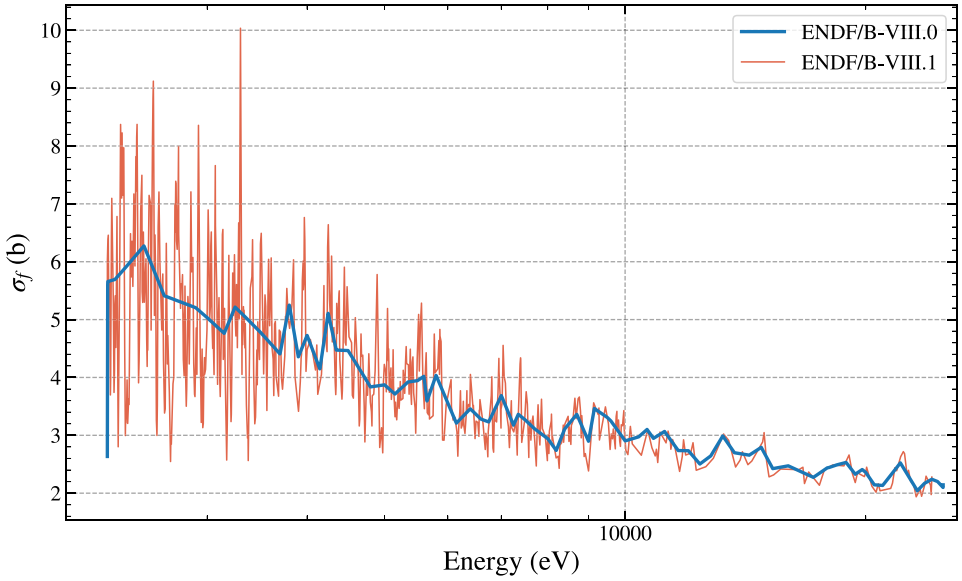

Fig. 2. ^{235}U fission cross section in the URR for ENDF/B-VIII.0 and ENDF/B-VIII.1, both derived from the Weston and Todd [17] measurement but with different degrees of smoothing.

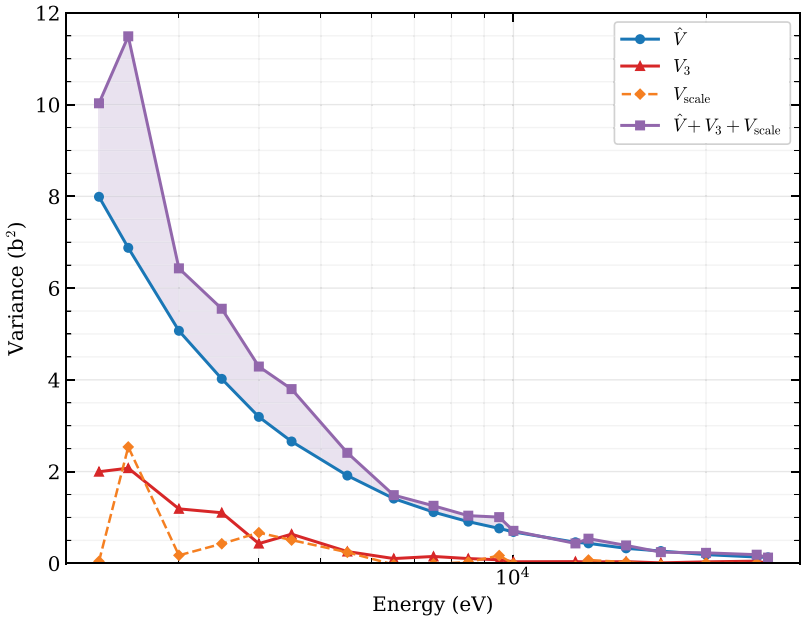

Fig. 3. Variance decomposition of the ^{235}U fission cross section across the URR (ENDF/B-VIII.1). $\hat{V}$: estimated fluctuation variance from PURR ladder sampling. V_3: file 3 variance. V_{scale}: scaling-induced variance from `LSSF = 1` multiplicative normalization. The shaded region between $\hat{V}$ and $\hat{V} + V_3 + V_{\text{scale}}$ represents the total variance overcounting seen by transport codes.

structure of $\bar{\sigma}$. The variance-preserving methodology derived in the next section addresses both through a unified affine transformation framework.

III. VARIANCE-PRESERVING METHODOLOGY AND IMPLEMENTATION

This section derives the variance-preserving transformations and describes their implementation in the NJOY/PURR processing code.

III.A. Mean Correction with Variance Preservation

Given a sampled probability table distribution $\{\sigma_j, P_j\}$ with mean $\hat{\mu}$ and variance $\hat{V}$, the goal is to determine a transformed set $\{\sigma'_j\}$ such that

$$\sum_j P_j \sigma'_j = \bar{\sigma} \ , \tag{13}$$

and

$$\sum_j P_j (\sigma'_j - \bar{\sigma})^2 = \hat{V} \ . \tag{14}$$

Variance is invariant under additive shifts. Therefore, the minimal correction that enforces Eq. (13) while preserving Eq. (14) is

$$\sigma'_j = \sigma_j + \Delta \ , \tag{15}$$

with

$$\Delta = \bar{\sigma} - \hat{\mu} \ . \tag{16}$$

This guarantees that the transformed distribution has mean $\bar{\sigma}$ and retains $\hat{V}$.

If factors are preferred for storage, the equivalent corrected factors are

$$f'_j \equiv \frac{\sigma'_j}{\bar{\sigma}} = \frac{\sigma_j + (\bar{\sigma} - \hat{\mu})}{\bar{\sigma}} \ , \tag{17}$$

which still satisfies $\sum_j P_j f'_j = 1$.

III.B. Variance Budget with Within-Bin Structure

The correction above assumes that the entire within-bin variance relevant to self-shielding should be represented by the probability table. In some applications, one may wish to retain within-bin structure in $\bar{\sigma}$ while also representing additional unresolved fluctuations via probability table sampling. In that case, variance can be double counted unless a variance budget is enforced.

Let $\hat{V}$ continue to denote the estimated fluctuation variance as defined in Eq. (10). Let V_3 be the within-bin

variance of $\bar{\sigma}$. Now, the target is a residual probability table variance V_{PT} satisfying

$$\hat{V} = V_{\mathrm{PT}} + V_3 \ , \tag{18}$$

neglecting a covariance term between the two components (discussed below). Therefore,

$$V_{\mathrm{PT}} = \hat{V} - V_3 \ . \tag{19}$$

This is resolved by performing an affine transform of the sampled distribution:

$$\sigma'_j = a\,\sigma_j + b \ . \tag{20}$$

Because adding b does not affect variance,

$$\mathrm{Var}(\sigma') = a^2 \hat{V} \ . \tag{21}$$

To enforce $\mathrm{Var}(\sigma') = V_{\mathrm{PT}}$, we require

$$a = \sqrt{1 - \frac{V_3}{\hat{V}}} \ . \tag{22}$$

The constant b is set by enforcing the correct mean:

$$\sum_j P_j \sigma'_j = a\hat{\mu} + b = \bar{\sigma} \quad \Rightarrow \quad b = \bar{\sigma} - a\hat{\mu} \ . \tag{23}$$

Combining Eqs. (22) and (23), the variance-budgeted probability table entries are

$$\sigma'_j = \bar{\sigma} + a(\sigma_j - \hat{\mu}), \qquad a = \sqrt{1 - \frac{V_3}{\hat{V}}} \ . \tag{24}$$

In factor form,

$$f'_j = \frac{\sigma'_j}{\bar{\sigma}} = 1 + \frac{a}{\bar{\sigma}}(\sigma_j - \hat{\mu}) \ . \tag{25}$$

Eq. (18) neglects the covariance between the unresolved component and $\bar{\sigma}$. In practice, estimating such a covariance requires attributing which structures in $\bar{\sigma}$ correspond to structures in the ladder ensemble, information that is generally inaccessible in the unresolved regime. The variance-budgeting form above is therefore intended as a practical, controllable approximation.

Note that Eq. (24) subsumes the pure mean-shift correction of Eqs. (15) and (16) as the limiting case $V_3 = 0$ (i.e., $a = 1$). The two problems identified in Sec. II are thus addressed by a single affine framework, with the value a controlling the degree of variance reduction.

III.C. Implementation in NJOY/PURR

The variance-budgeting methodology is implemented as a fork [18] of the PURR module in NJOY2016 [3]. Two modifications are required: computing V_3 for each reaction at each probability table energy grid point, and applying the per-reaction scaling parameter a during factor generation.

III.C.1. Computing Within-Bin File 3 Variance

The probability table energy grid $\{E_1, E_2, \ldots, E_N\}$ defines N grid points at which PURR generates probability tables via statistical ladder sampling. Because different reactions may carry very different degrees of structure in the File 3 cross section, V_3 must be evaluated at each grid point for each reaction channel r (total, elastic, fission, capture) independently. For ^{235}U, for example, the elastic and capture cross sections are essentially smooth in the URR in both the ENDF/BVIII.0 and ENDF/BVIII.1 evaluations ($V_{3,r} \approx 0$ for their respective channels), while the fission cross section exhibits significant resonant structure ($V_{3,r} > 0$).

For each grid point E_i, the relevant energy window is defined using geometric midpoints between adjacent grid points:

$$E_{i-\frac{1}{2}} = \sqrt{E_{i-1}\,E_i}, \qquad E_{i+\frac{1}{2}} = \sqrt{E_i\,E_{i+1}} \ . \tag{26}$$

The use of geometric (rather than arithmetic) midpoints is appropriate because the URR grid points are approximately logarithmically spaced. $V_{3,r}$ is then computed by densely sampling $\bar{\sigma}_r$ at M uniformly spaced subpoints within $[E_{i-1/2}, E_{i+1/2}]$:

$$V_{3,r}(E_i) = \frac{1}{M}\sum_{m=1}^{M} \bar{\sigma}_r^2(E_m) - \left(\frac{1}{M}\sum_{m=1}^{M} \bar{\sigma}_r(E_m)\right)^2, \tag{27}$$

where $\bar{\sigma}_r(E_m)$ is the evaluated cross section for reaction r at energy E_m obtained via the standard ENDF interpolation law. The implementation described in this work uses $M = 200$, which provides adequate resolution for cross sections with resonant structure comparable to or broader than the average level spacing in the URR.

At the URR boundaries, one-sided intervals are used:

$$\begin{aligned} &\text{Firstpoint}: \quad [E_1,\ E_{3/2}]\ , \\ &\text{Lastpoint}: \quad [E_{N-\frac{1}{2}},\ E_N]\ . \end{aligned} \tag{28}$$

This avoids extrapolation outside the URR while still providing a local estimate of V_3 at the boundary grid points. In practice, the first grid point at the RRR/URR transition is the most sensitive to this choice since it represents the least statistical portion of the URR. More sophisticated approaches, such as incorporating resolved-range pointwise data from the PENDF tape below E_1, would improve the edge treatment but add significant implementation complexity.

III.C.2. Per-Reaction Variance-Budget Parameter

At each grid point E_i, the sampled probability table variance for reaction r is

$$\hat{V}_r(E_i) = \sum_{j=1}^{N_{\text{bin}}} P_j \left(\sigma_{j,r} - \hat{\mu}_r\right)^2 , \tag{29}$$

where $\sigma_{j,r}$ and P_j are the bin-averaged cross section and probability for bin j from the PURR ladder sampling, respectively, and $\hat{\mu}_r = \sum_j P_j \sigma_{j,r}$ is the sampled mean. The variance-budgeting parameter for reaction r at grid point E_i is then

$$a_r(E_i) = \begin{cases} \sqrt{1 - V_{3,r}(E_i)/\hat{V}_r(E_i)} & \text{if } \hat{V}_r > 0 \text{ and } V_{3,r} < \hat{V}_r\ , \\ 0 & \text{if } \hat{V}_r > 0 \text{ and } V_{3,r} \geq \hat{V}_r\ , \\ 1 & \text{if } \hat{V}_r = 0\ . \end{cases} \tag{30}$$

The case $V_{3,r} \geq \hat{V}_r$ corresponds to $\bar{\sigma}_r$ carrying at least as much within-bin variance as the sampled distribution, which would make a imaginary. In that regime, the probability table should contribute no additional fluctuation variance for that reaction, and $a_r = 0$ sets the probability table factor to 1.

The corrected probability table factors are then reaction specific:

$$f'_{j,r} = 1 + \frac{a_r}{\bar{\sigma}_r}\left(\sigma_{j,r} - \hat{\mu}_r\right) , \tag{31}$$

where $\bar{\sigma}_r$ is the evaluated mean for reaction r at E_i. The output remains in standard `LSSF = 1` format, preserving compatibility with existing transport codes. The only change is the numerical values of the factors, which now encode per-reaction variance budgeting rather than a uniform multiplicative scaling. For evaluations where $\bar{\sigma}_r$ is smooth ($V_{3,r} \approx 0$ for all r), $a_r \approx 1$ for all reactions, and the method reduces to the pure additive-shift correction of Eqs. (15) and (16).

IV. VALIDATION

IV.A. Self-Consistency of the Variance Decomposition

The variance-budgeting methodology rests on the claim that the total fluctuation variance $\hat{V}$ can be separated into a File 3 component V_3 and a residual probability table component $\hat{V} - V_3$, with no change to the self-shielding seen by transport. This subsection tests that claim directly. The test is one of internal self-consistency: No experimental observable is used as a reference. Instead, the bin-averaged transmission is computed under five cases that differ in how the total variance is distributed between the probability table and $\bar{\sigma}$, and the results are compared to one another. If the variance decomposition of Eq. (18) is valid, transferring variance from the probability table into $\bar{\sigma}$ (or vice versa) should leave the computed transmission unchanged.

Transmission is chosen as the test observable because it isolates the variance-driven self-shielding effect. For a thick sample, the nonlinearity of $\exp(-n\sigma)$ makes the bin-averaged transmission sensitive to the full within-bin distribution of cross-section values [Eq. (4)]. Differential reaction rate measurements (e.g., fission cross sections measured with thin foils or fission chambers) operate in a regime where $n\sigma \ll 1$ and the transmission is essentially linear in σ, making them insensitive to fluctuation variance.

To stress-test the decomposition, a deliberately extreme $\bar{\sigma}$ is constructed from the highly resolved total cross section reported by Harvey et al. [19], an enriched ^{235}U transmission measurement performed at the Oak Ridge Electron Linear Accelerator. This experimental cross section is used solely as a structured input, not as a reference for comparison. It provides a much larger V_3 than would occur in any realistic evaluation, making the test a stringent validation of the decomposition under worst-case conditions. The fine-grid $\bar{\sigma}$ is applied over the same coarse energy binning used in the transmission calculation, and the probability table variance is reduced by the factor $a = \sqrt{1 - V_3/\hat{V}}$ at each grid point.

All five cases use the same PURR probability table output, generated from the ENDF/B-VIII.1 average resonance parameters. The cases differ only in how the probability table factors are applied and in the degree of

structure retained in $\bar{\sigma}$. Five cases are compared: (i) coarse $\bar{\sigma}$ with full probability table sampling (the reference since all variance resides in the probability table), (ii) coarse $\bar{\sigma}$ with no probability table treatment (un-self-shielded), (iii) fine-grid $\bar{\sigma}$ with no probability table treatment (partial self-shielding from $\bar{\sigma}$ structure alone), (iv) fine-grid $\bar{\sigma}$ with variance-budgeted probability table sampling (the method under test), and (v) fine-grid $\bar{\sigma}$ with full, unmodified probability table sampling (double counting).

Fig. 4 illustrates the fine-grid versus coarse representation of the ^{235}U cross section used in the test, along with the corresponding variance-budget parameter $a(E)$. Bins with significant within-bin structure in $\bar{\sigma}$ yield smaller a, indicating that the probability table variance is reduced to avoid double counting variance already present in $\bar{\sigma}$.

The transmission results are shown in Fig. 5. The central result is that the variance-budgeted case (iv) reproduces the reference case (i) to within 0.02%, confirming that the decomposition $\hat{V} = (\hat{V} - V_3) + V_3$ holds at the level of the observable. The success of this decomposition under the deliberately extreme $\bar{\sigma}$ used here provides confidence that it will hold for the more moderate structure present in the ENDF/B-VIII.1 fission evaluation. The alternative treatments remain distinctly separated: Omitting probability tables (cases ii and iii) underestimates self-shielding, while applying the full probability table on top of the structured $\bar{\sigma}$ (case v,

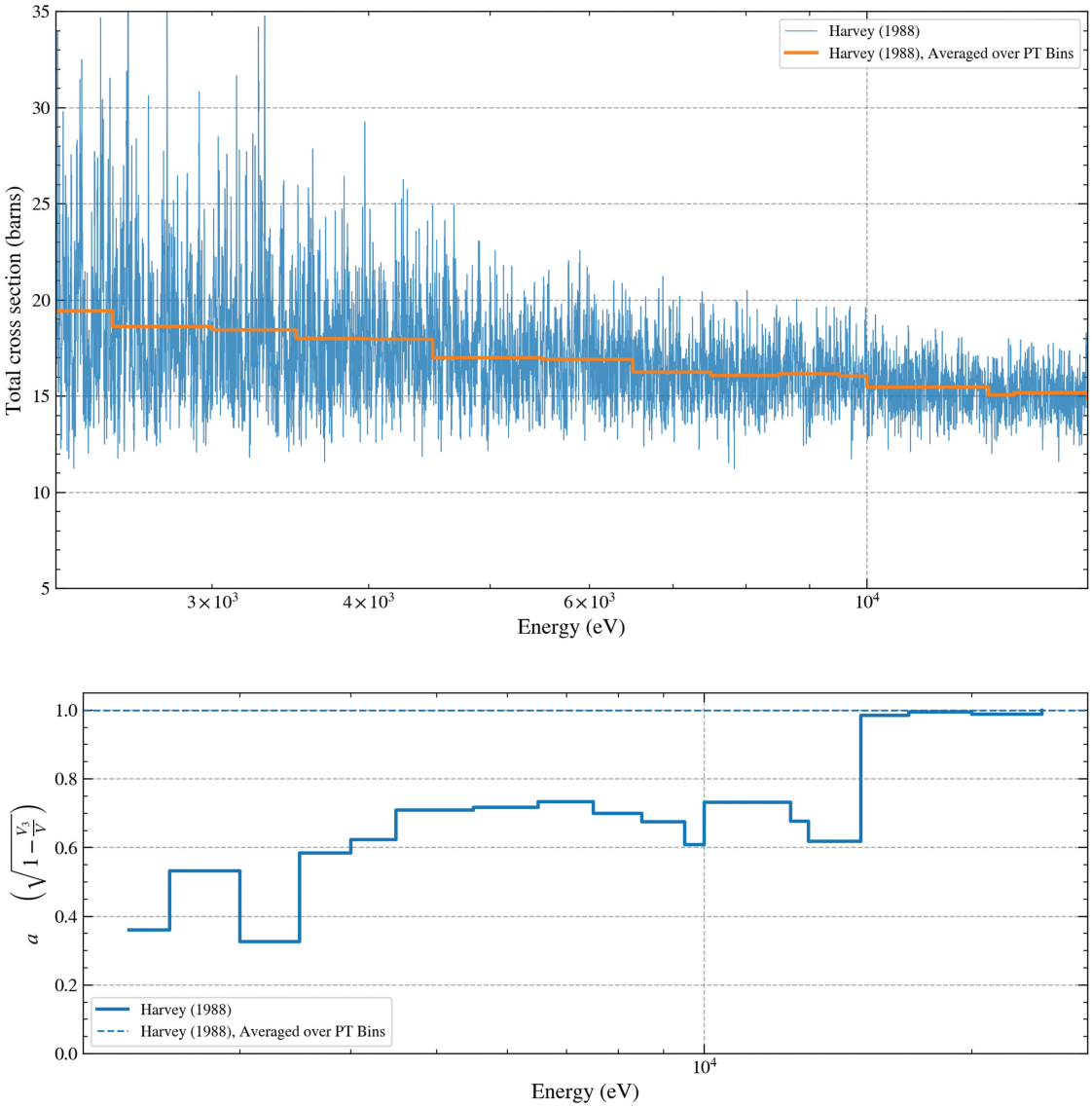

Fig. 4. Controlled ^{235}U transmission demonstration inputs. (Top) Fine-grid $\bar{\sigma}$ from the Harvey et al. [19] experimental transmission measurement and its coarse bin-averaged representation over the probability table (PURR) energy boundaries. (Bottom) Variance-budget parameter $a(E) = \sqrt{1 - V_3/\hat{V}}$ evaluated in each probability table bin.

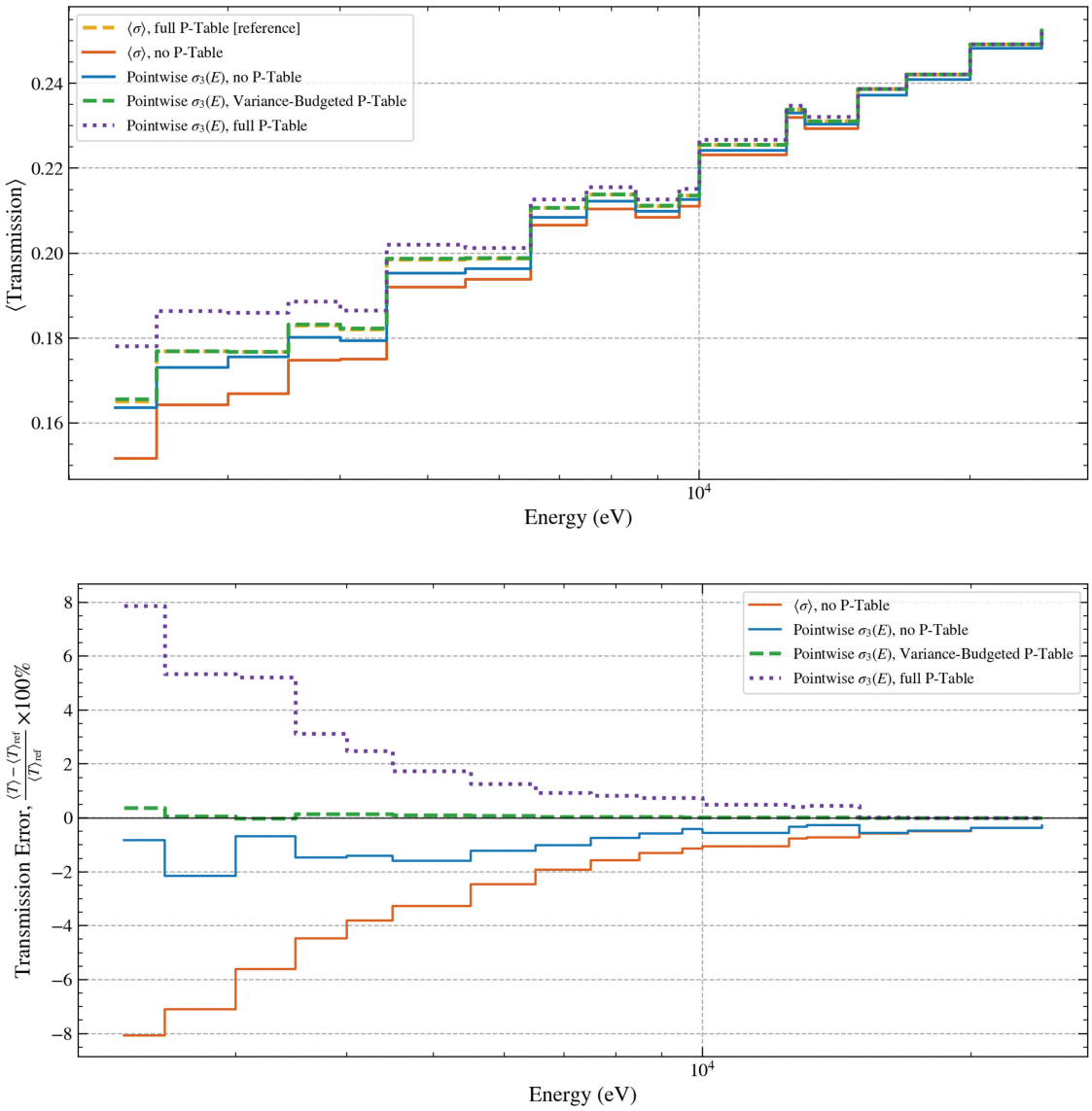

Fig. 5. Transmission comparison for the controlled ^{235}U self-consistency test. (Top) Bin-averaged transmissions for the five cases described in the text. (Bottom) Transmission ratios relative to the reference case (i), T/T_{ref}, highlighting the bias introduced by neglecting probability tables or by double counting fluctuations.

double counting) overestimates it. The variance-budgeted treatment is the only case that preserves the reference transmission while permitting $\bar{\sigma}$ to carry energy-dependent structure within the probability table bins.

To quantify this agreement, Table 1 reports the root-mean-square (RMS), mean bias, and maximum absolute deviation of the binned transmissions relative to case (i), which serves as the computational reference. Over 2.25 to 15 keV, the variance-budgeted method reduces the RMS deviation by nearly an order of magnitude compared to using the fine-grid $\bar{\sigma}$ without probability tables, while simultaneously avoiding the large deviations observed for the double-counting case.

An exception to the close agreement occurs in the first energy bin, where the variance-budgeted result exhibits a small but systematic deviation from the reference. This is expected: The first URR bin is closest to the RRR/URR transition, is most sensitive to bin-edge effects, and is therefore where any mismatch between a coarse probability table representation and the deliberately aggressive $\bar{\sigma}$ is most likely to appear. It should also be noted that the $\bar{\sigma}$ used here is constructed directly from reported experimental data with no additional processing, so the apparent within-bin variance may include statistical counting noise and residual systematic effects that exceed the physically meaningful fluctuation content. This matters because the

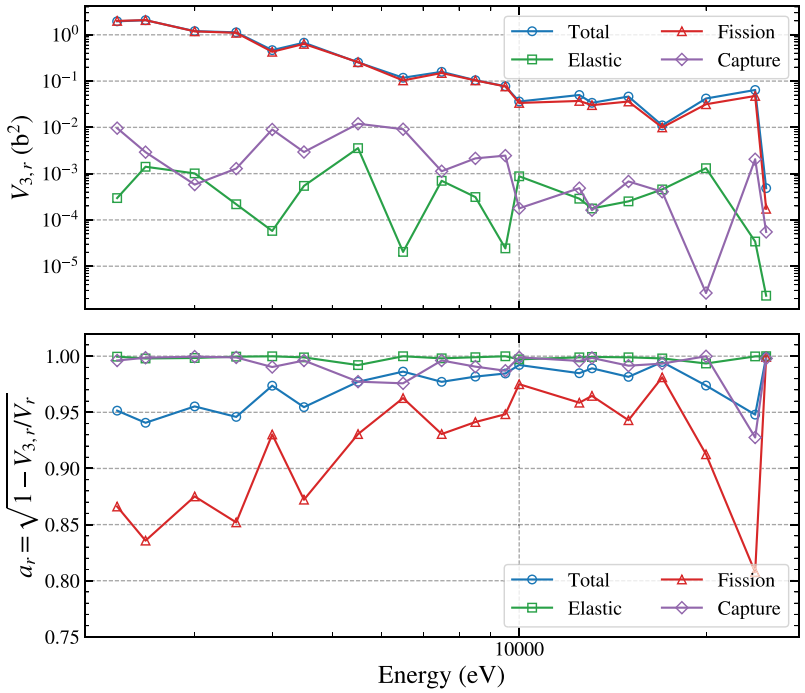

Fig. 6. Per-reaction variance budget for ^{235}U (ENDF/B-VIII.1). (Top) File 3 variance $V_{3,r}$ for total, elastic, fission, and capture channels at each PURR energy grid point. The fission channel dominates by two to three orders of magnitude over the elastic and capture channels, and the total cross section V_3 closely tracks fission. (Bottom) Variance-budget parameter $a_r = \sqrt{1 - V_{3,r}/\hat{V}_r}$ for each reaction channel. Fission requires the largest correction ($a_{\text{fis}} \approx 0.83$ to 0.95), while elastic and capture remain near 1.

TABLE 1

Agreement of Bin-Averaged Transmissions in the Controlled ^{235}U Self-Consistency Test Over 2.25 to 15 keV*

Method	RMS	Mean Bias	Maximum Absolute Difference
(i) $\bar{\sigma}$, full P-Table [reference]	0	0	0
(ii) $\bar{\sigma}$, no P-Table	6.109e−03	−4.719e−03	1.332e−02
(iii) Fine-grid $\bar{\sigma}$, no P-Table	1.884e−03	−1.660e−03	3.805e−03
(iv) Fine-grid $\bar{\sigma}$, variance-budgeted P-Table	1.859e−04	1.109e−04	6.165e−04
(v) Fine-grid $\bar{\sigma}$, full P-Table	4.882e−03	3.224e−03	1.298e−02

*Case (i), the coarse $\bar{\sigma}$ with full probability table sampling, is used as the computational reference.

variance-budgeting factor [Eq. (22)] would become imaginary if $V_3 > \hat{V}$, which is nonphysical. Nevertheless, even under this deliberately pathological input, the variance-budgeted treatment reduces the RMS transmission error by nearly an order of magnitude relative to all other methods (Table 1), confirming that the approach remains robust well beyond the regime of practical interest.

IV.B. Per-Reaction Variance Budget for ^{235}U

With the variance decomposition validated, the per-reaction implementation (Sec. III.C.2) is applied to the ENDF/B-VIII.1 ^{235}U evaluation. Fig. 6 presents $V_{3,r}$ and a_r for all four reaction channels at each PURR grid point.

The top panel of Fig. 6 confirms that V_3 is overwhelmingly concentrated in the fission channel: $V_{3,\text{fis}}$ exceeds $V_{3,\text{el}}$ and $V_{3,\text{cap}}$ by two to three orders of magnitude across the URR. The total $V_{3,\text{tot}}$ closely tracks $V_{3,\text{fis}}$, which is expected since $\sigma_{\text{tot}} = \sigma_{\text{el}} + \sigma_{\text{fis}} + \sigma_{\text{cap}}$ and the within-bin variance of the sum is dominated by whichever partial carries structure; in this evaluation, that is exclusively the fission channel.

The bottom panel of Fig. 6 shows the resulting per-reaction a_r values. The fission parameter a_{fis} ranges from approximately 0.83 at the lowest URR energies to 0.95 at intermediate energies, indicating that the probability table

modulation amplitude must be reduced by 5% to 17% to preserve the sampled fission variance $\hat{V}_{\mathrm{fis}}$, and account for the $V_{3,\mathrm{fis}}$ contribution. The total channel tracks fission but with smaller corrections because the elastic and capture partials (which carry negligible V_3) dilute the fission contribution when summed. The elastic and capture channels themselves require essentially no correction ($a_r \approx 1$).

It is worth contrasting these values with the deliberately extreme validation case of Sec. IV.A, where the highly resolved $\bar{\sigma}$ drove a below 0.4 in several bins. The ^{235}U fission evaluation represents a much more moderate regime: The corrections are significant enough to produce a measurable bias in integral benchmarks (Sec. IV.C) but mild enough that the variance decomposition of Eq. (18) is well within its domain of validity.

As shown earlier in Fig. 1, $\bar{\sigma}_{\mathrm{fis}}$ and $\hat{\mu}_{\mathrm{fis}}$ also diverge systematically, confirming that the multiplicative scaling of Problem 1 applies nontrivially to the fission channel. The full variance decomposition (Fig. 3) shows that the combined overcounting from both mechanisms exceeds 40% of $\hat{V}$ at the lowest URR energies. The per-reaction nature of the variance budget is essential: Computing $V_{3,r}$ and a_r independently for each reaction channel correctly identifies the fission partial as the source of the double-counting problem and applies the appropriate correction without affecting the elastic or capture channels.

IV.C. Critical Benchmark Results

Integral transport calculations are performed with MCNP 6.3 [20]. The selected benchmark is HEU-MET-INTER-011 [21,22], a highly enriched ^{235}U configuration with intermediate-spectrum leakage (designed to be sensitive to URR self-shielding treatments). In each case, the ACE-format cross sections are generated with NJOY2016 [3]. All other isotopes in the problem are left unchanged between runs so that differences in reactivity can be attributed directly to the ^{235}U probability table treatment.

Table 2 compares five cases from the benchmark suite, spanning a range of experimental geometries. For each case, three calculations are performed: ENDF/B-VIII.1 with probability tables disabled, with the standard `LSSF = 1` treatment, and with variance-preserved processing. The eigenvalue obtained with probability tables disabled is denoted $k_{\mathrm{eff}}^{\mathrm{off}}$ and serves as the un-self-shielded baseline. The self-shielding reactivity worth is defined as the reactivity depression relative to this baseline: $\Delta\rho_{\mathrm{LSSF}}$ for the standard treatment and $\Delta\rho_{\mathrm{VP}}$ for the variance-preserved treatment. Both are negative, reflecting the self-shielding depression of reactivity. All MCNP statistical uncertainties are ±0.00002 in k_{eff}.

In all five cases, both the standard and variance-preserved treatments yield negative self-shielding worth relative to the un-self-shielded baseline, indicating that URR probability table sampling reduces reactivity in this benchmark configuration. The variance-preserved treatment yields a self-shielding worth of −48 to −65 pcm, while the standard `LSSF = 1` method produces −76 to −92 pcm, consistently larger in magnitude by a factor of approximately 1.5. Because the variance-preserved result reflects the self-shielding implied by $\hat{V}$ without artificial inflation from V_{scale} or double counting of V_3, the difference is attributable entirely to the overcounting identified in Secs. II.C and III.B.

This overprediction has implications for evaluation practice. When URR average resonance parameters are adjusted to reproduce integral benchmarks under the standard `LSSF = 1` workflow, the tuned parameters are implicitly compensating for the inflated self-shielding. The evaluation reproduces the correct k_{eff} but through parameters whose self-shielding influence is amplified

TABLE 2

Self-Shielding Reactivity Worth for HEU-MET-INTER-011*

Case	$k_{\mathrm{eff}}^{\mathrm{off}}$	$\Delta\rho_{\mathrm{VP}}$ (pcm)	$\Delta\rho_{\mathrm{LSSF}}$ (pcm)	$\Delta\rho_{\mathrm{LSSF}}/\Delta\rho_{\mathrm{VP}}$
i	1.00829	−48	−76	158%
ii	1.00749	−57	−85	149%
iii	1.00631	−64	−89	139%
iv	1.00584	−58	−88	152%
v	1.00335	−65	−92	142%

*$k_{\mathrm{eff}}^{\mathrm{off}}$ is the eigenvalue with probability tables disabled (un-self-shielded baseline). $\Delta\rho_{\mathrm{VP}}$ and $\Delta\rho_{\mathrm{LSSF}}$ are the reactivity depressions relative to this baseline for the variance-preserved and standard `LSSF = 1` treatments, respectively. The ratio $\Delta\rho_{\mathrm{LSSF}}/\Delta\rho_{\mathrm{VP}}$ quantifies the overprediction of self-shielding by the standard method. All k_{eff} uncertainties are ±0.00002.

by ~50% relative to the physical compound-nucleus statistics. This point is discussed further in Sec. V.A.

Because the only change between the standard and variance-preserved cases is the ^{235}U probability table scaling procedure, the consistent overprediction factor across all five configurations supports the interpretation that the effect is systematic rather than configuration specific.

V. DISCUSSION

V.A. Backward Compatibility and Tuned Parameters

Many evaluations and processed libraries have been produced, validated, and in some cases benchmark-tuned under the historical `LSSF = 1` workflow. For most production evaluations, where $\bar{\sigma}$ is smooth ($V_3 \approx 0$) and $\bar{\sigma} \approx \hat{\mu}$, the standard factor method behaves as intended. If $V_3 \approx 0$, then $a \to 1$, and Eq. (24) reduces to the pure mean shift of Eqs. (15) and (16). If additionally, $\bar{\sigma} = \hat{\mu}$, then $f_j' = \sigma_j/\hat{\mu}$, recovering the original factor definition [Eq. (11)].

However, the benchmark results of Sec. IV.C show that for the ENDF/B-VIII.1 ^{235}U evaluation, the standard `LSSF = 1` method overpredicts the self-shielding reactivity worth by approximately 150% relative to the variance-preserved result. This raises a serious concern for evaluation practice: When URR average resonance parameters are adjusted to reproduce integral benchmarks under the standard workflow, the tuned parameters must compensate for this inflated self-shielding. The resulting parameters reproduce the correct k_{eff}, but their self-shielding influence is amplified by ~50% beyond what the underlying compound-nucleus statistics would produce. The evaluation "works" in the sense of matching benchmarks through compensating errors, but the physical interpretation of the tuned parameters is compromised: They are partially absorbing a processing artifact rather than purely representing the nuclear physics.

Retroactively applying variance-preserving corrections to such an evaluation would degrade benchmark agreement without improving the underlying physics. For this reason, the variance-preserving transformations should be treated as a forward-looking option for new evaluations. A straightforward implementation path is to introduce a new switch (e.g., `LSSF = 2`) that explicitly requests variance-preserving reconstruction while keeping `LSSF = 1` behavior unchanged for legacy data [16,23].

V.B. Implications for URR Covariance Representations

The independence of V from $\bar{\sigma}$ (Sec. II.A) has a direct implication for how URR uncertainties should be represented in evaluated data. In the ENDF format, uncertainties on the average resonance parameters are stored in File 32, while uncertainties on the pointwise cross sections are stored in File 33. If V and $\bar{\sigma}$ are physically independent quantities, then their uncertainty representations should not be treated as interchangeable: File 32 should encode uncertainty in the compound-nucleus fluctuation content, while File 33 should encode uncertainty in the mean cross section, which may include nonfluctuating components.

Recent work [24] has sought to enforce consistency between File 32 and File 33 by requiring that the two representations produce equivalent cross-section uncertainties in the URR. While this equivalence is a useful constraint that reduces the number of independent parameters in the evaluation, the analysis of Sec. II.A suggests it rests on an assumption that does not hold generally. When the mean cross section includes contributions from non-compound-nucleus mechanisms, e.g., direct capture, inelastic scattering, doorway states, and other smooth components, the uncertainty on the mean is not equivalent to the uncertainty on the fluctuation content. Equating File 32 and File 33 uncertainties implicitly assumes that the entire cross section is governed by compound-nucleus statistics, which is precisely the assumption that the variance-preserving framework relaxes. Treating File 32 and File 33 as independent representations while introducing an additional free parameter more faithfully reflects the physical decoupling between the mean and variance in the URR.

V.C. Enabling Structured URR Representations

A long-standing tension in URR evaluation is the treatment of observable resonances that fall within the unresolved range. When experimental resolution permits some individual resonances to be identified but not all, the evaluator faces an unsatisfying choice: Extend the RRR boundary upward, risking incomplete level assignments and missing-level bias, or discard the observable structure and begin the URR with a smooth File 3, losing information that was experimentally obtained.

The variance-budgeting framework offers a resolution. An evaluator can include observed resonant structure in $\bar{\sigma}$ within the URR, and the processing code will automatically reduce the probability table modulation to avoid double counting V_3. As mentioned previously in Sec. II.D, the ENDF-6 manual has historically cautioned against

introducing significant structure into File 3 in the URR [16] precisely because the standard `LSSF = 1` workflow has no mechanism to account for it. The variance budget removes this restriction. The evaluator is free to retain whatever structure is physically justified, and the affine transform of Eq. (24) distributes $\hat{V}$ between the probability table and $\bar{\sigma}$ accordingly.

This also addresses the inter-isotope coupling problem. Strong resonances in one isotope can create energy-correlated flux depressions (resonance shadows [25]) and windows [26] that affect the effective cross sections of neighboring isotopes. Independent probability table sampling erases this coupling [27]. Retaining physically meaningful structure in File 3, now possible without variance double counting, allows the transport solver to capture these cross-isotope energy-correlated effects while the probability table supplies only the residual V_{PT}.

V.D. Processing Limitations

A practical limitation of retaining structured pointwise data in the URR is that industry-standard processing workflows do not Doppler-broaden unresolved-range pointwise structure; only the probability tables themselves receive temperature-dependent treatment [28,29]. Resonant structure in File 3 would therefore be representative only of the measurement temperature and would not transfer correctly to reactor operating conditions. Extending Doppler broadening to structured URR pointwise data is a processing code development that would need to accompany any widespread adoption of structured File 3 representations in the URR.

VI. CONCLUSIONS

Probability tables remain a practical technique for representing URR self-shielding effects in Monte Carlo neutron transport. However, to maintain physical fidelity, they must preserve the estimated variance $\hat{V}$. This paper has identified two mechanisms by which standard processing can distort $\hat{V}$: multiplicative mean enforcement (which introduces the scaling-induced variance V_{scale}) and File 3 variance double counting (which adds V_3). An affine transformation has been derived that addresses both.

The common practice of enforcing mean consistency via multiplicative renormalization inadvertently rescales the sampled distribution and biases self-shielding. A variance-preserving correction follows naturally: Enforce the evaluated mean $\bar{\sigma}$ via an additive shift (or, when retaining within-bin structure, a variance-budgeted affine transform) without altering $\hat{V}$.

This issue has become practically relevant with the ENDF/B-VIII.1 evaluation of ^{235}U, which introduced substantial fission cross-section structure in the URR derived from the Weston and Todd [17] measurement. A detailed variance decomposition (Fig. 3) shows that the combined overcounting from both mechanisms exceeds 40% of $\hat{V}$ at the lowest URR energies. The per-reaction variance-budgeting methodology developed here, implemented in the PURR module of NJOY2016 (Sec. III.C), addresses this by computing $V_{3,r}$ independently for each reaction and reducing the probability table modulation accordingly. This has all been done within the existing `LSSF = 1` factor format, requiring no changes to transport codes.

Through controlled transmission tests, the variance decomposition has been validated under a deliberately extreme test case. Integral benchmark calculations using the HEU-MET-INTERM-011 suite demonstrate that the standard `LSSF = 1` processing overpredicts the URR self-shielding reactivity worth by approximately 150% relative to the variance-preserved result, confirming that the artifact is both systematic and quantitatively significant. Beyond correcting this specific issue, the variance-budgeting framework enables a new class of URR evaluations in which physically meaningful structure can be retained in $\bar{\sigma}$ without double counting the cross-section variance.

Author Contributions

CRediT: **Alec Golas:** Conceptualization, Formal analysis, Investigation, Methodology, Software, Validation, Visualization, Writing – original draft, Writing – review & editing; **Y. Danon:** Funding acquisition, Project administration, Supervision, Writing – review & editing; **A. M. Lewis:** Conceptualization, Validation, Writing – review & editing; **D. Barry:** Validation, Writing – review & editing.

Disclosure Statement

No potential conflict of interest was reported by the author(s).

Funding

The work was supported by the U.S. Department of Energy, National Nuclear Security Administration, through the Nuclear Criticality Safety Program.

ORCID

Alec Golas http://orcid.org/0000-0003-2332-7957

References

1. D. Brown et al., "ENDF/B-VIII.0: The 8th Major Release of the Nuclear Reaction Data Library with CIELO-Project Cross Sections, New Standards and Thermal Scattering Data," *Nucl. Data Sheets*, **148**, 1 (2018); https://doi.org/10.1016/j.nds.2018.02.001.
2. G. P. A. Nobre et al., "ENDF/B-VIII.1: Updated Nuclear Reaction Data Library for Science and Applications," *Nucl. Data Sheets*, **210**, 1 (2026); https://doi.org/10.1016/j.nds.2026.04.001.
3. R. Macfarlane et al., "The NJOY Nuclear Data Processing System, Version 2016," LA-UR-17-20093, Los Alamos National Laboratory (2017).
4. D. E. Cullen, "A Short History of ENDF/B Unresolved Resonance Parameters," LLNL-TR-461199 (ENDF-369), Lawrence Livermore National Laboratory (2010).
5. J.-C. Sublet et al., "Unresolved Resonance Range Cross Section, Probability Tables, and Self-Shielding Factors," CEA-R-6227, Commissariat à l'Énergie Atomique (2009).
6. F. H. Fröhner, "SESH: A Fortran IV Code for Calculating the Self-Shielding and Multiple Scattering Effects for Neutron Cross Section Data Interpretation in the Unresolved Resonance Region," GA-8380, General Atomics (1968).
7. W. Rudin, *Real and Complex Analysis*, 3rd ed., McGraw-Hill, New York, NY (1987).
8. M. Kawai, A. K. Kerman, and K. W. McVoy, "Modification of Hauser-Feshbach Calculations by Direct-Reaction Channel Coupling," *Ann. Phys.*, **75**, *1*, 156 (1973); https://doi.org/10.1016/0003-4916(73)90465-X.
9. B. V. Carlson, J. E. Escher, and M. S. Hussein, "Theoretical Descriptions of Compound-Nuclear Reactions: Open Problems and Challenges," *J. Phys. G*, **41**, *9*, 094003 (2014); https://doi.org/10.1088/0954-3899/41/9/094003.
10. G. Mantzouranis, "Direct and Compound Contributions to (n,γ) Cross Sections," *Z. Phys.*, **264**, *5*, 405 (1973); https://doi.org/10.1007/BF01391709.
11. A. Lindholm et al., "Direct-Semidirect and Compound Contributions to Radiative Neutron Capture Cross Sections," *Nucl. Phys. A*, **339**, 205 (1980); https://doi.org/10.1016/0375-9474(80)90087-1.
12. K. H. Guber et al., "Astrophysical Reaction Rates for ^{58,60}Ni(n,γ) from New Neutron Capture Cross Section Measurements," *Phys. Rev. C.*, **82**, *5*, 057601 (2010); https://doi.org/10.1103/PhysRevC.82.057601.
13. V. M. Maslov et al., "Evaluation of the Unresolved Resonance Range of ^{238}U," *Ann. Nucl. Energy*, **29**, *14*, 2107 (2002); https://doi.org/10.1016/s0306-4549(02)00005-1.
14. H. Feshbach, A. K. Kerman, and R. H. Lemmer, "Intermediate Structure and Doorway States in Nuclear Reactions," *Ann. Phys.*, **41**, *2*, 230 (1967); https://doi.org/10.1016/0003-4916(67)90235-7.
15. L. B. Levitt, "The Probability Table Method for Treating Unresolved Neutron Resonances in Monte Carlo Calculations," *Nucl. Sci. Eng.*, **49**, *4*, 450 (1972); https://doi.org/10.13182/NSE72-3.
16. M. Herman et al., "ENDF-6 Formats Manual: Data Formats and Procedures for the Evaluated Nuclear Data Files ENDF/B-VI and ENDF/B-VII," BNL-90365-2009 Rev.1, ENDF-102, Brookhaven National Laboratory (2010).
17. L. W. Weston and J. H. Todd, "High-Resolution Fission Cross-Section Measurements of ^{235}U and ^{239}Pu," *Nucl. Sci. Eng.*, **111**, *4*, 415 (1992); https://doi.org/10.13182/NSE92-A15488.
18. A. Golas, "Variance-Preserving PURR Implementation (NJOY2016 Fork)," GitHub (2025); https://github.com/golasa97/NJOY2016.
19. J. A. Harvey et al., "High Resolution Transmission Measurements on ^{235}U, ^{239}Pu, and ^{238}U," Oak Ridge National Laboratory (1988).
20. J. A. Kulesza et al., "MCNP® Code Version 6.3.0 Theory & User Manual," LA-UR-22-30006, Rev. 1, Los Alamos National Laboratory (2022).
21. C. Percher et al., "The 2021 Edition of the ICSBEP Handbook," NEA No. 7592, Organisation for Economic Co-operation and Development, Nuclear Energy Agency (2022); https://www.oecd-nea.org/jcms/pl_20291.
22. T. Grove and T. Cutler, "Multiple Critical Unresolved Region Integral Experiment (MCURIE): A Proposed Integral Critical Experimental Framework for Unresolved Region and Intermediate Energies," Los Alamos National Laboratory (2023); https://www.osti.gov/biblio/2339539.
23. "Final Report of WPEC Subgroup 32: Assessment of the Unresolved Resonance Treatment for Cross Section and Covariance Representation," NEA/NSC/WPEC/DOC(2011)430, Organisation for Economic Co-operation and Development, Nuclear Energy Agency (2011); https://www.oecd-nea.org/jcms/pl_19042/final-report-of-wpec-subgroup-32.
24. D. Barry et al., "A New ^{103}Rh Unresolved Resonance Region Evaluation," *Ann. Nucl. Energy*, **188**, 109751 (2023); https://doi.org/10.1016/j.anucene.2023.109751.
25. I. Carlvik, "The Dancoff Correction in Lattice Calculations," AE-257, Aktiebolaget Atomenergi (Sweden) (1967); https://www.osti.gov/servlets/purl/4523167.
26. K. Furuta, Y. Oka, and S. Kondo, "Accuracy of Multi-Group Transport Calculation in D-T Fusion Neutronics," *J. Nucl. Sci. Technol.*, **24**, *4*, 333 (1987); https://doi.org/10.1080/18811248.1987.9735810.
27. M.-A. Descalle et al., "Implementation of Unresolved Resonance Region Probability Tables in the GNDS Format," LLNL-PROC-857166, Lawrence Livermore National Laboratory (2023); https://www.osti.gov/servlets/purl/2341964.

28. D. E. Cullen, "Doppler Broadening Update: Broadening Near the Unresolved Resonance Region," ENDF-370, LLNL-TR-534931, Lawrence Livermore National Laboratory (2012); https://www.nndc.bnl.gov/endfdocs/ENDF-370.pdf.

29. H. R. Trellue, R. C. Little, and M. B. Lee, "New ACE-Formatted Neutron and Proton Libraries Based on ENDF/B-VII.0," LA-UR-08-1999, Los Alamos National Laboratory (2008); https://nucleardata.lanl.gov/files/la-ur-08-1999.pdf.